KSCE Journal of Civil Engineering (2016) 20(4):1582-1593
DOI 10.1007/s12205-015-1560-0

Water Engineering
pISSN 1226-7988, eISSN 1976-3808
www.springer.com/12205

An Experimental Study of Mean and Turbulent Flow in a 180 Degree Sharp Open Channel Bend: Secondary Flow and Bed Shear Stress

Mohammad Vaghefi*, Maryam Akbari, and Ali Reza Fiouz*****

Received September 21, 2014/Revised February 23, 2015/Accepted June 10, 2015/Published Online August 7, 2015

Abstract

High flow velocity near the free surface in rivers is due to the presence of shear stress near the bed and its absence on the free surface. This phenomenon results in unsteadiness of the vertical velocity profile. Moreover, secondary flows in river bends cause velocity variations, accordingly leading to changes in shear stress near the bed. The present study evaluates and analyzes the effect of streamlines variations, maximum velocity distribution, and secondary flow strength on bed shear stress distribution along a 180 degree sharp bend built in the Hydraulic Laboratory of Persian Gulf University. Results suggest of the occurrence of maximum secondary flow strength at the second half of the bend. The evaluation of bed shear stress distribution using the TKE, modified TKE, and Reynolds methods at turbulent boundary layer demonstrated that the maximum shear stress occurred from the entrance of the bend to the bend apex area near the inner wall. Moreover, comparison of the Reynolds shear stress method at distances of 5 and 15% of the flow depth from the bed indicated that the maximum shear stress occurring at the lower layer moved from the 40 degree cross section to 60 degree cross section at the upper layer.

Keywords: *open channel flow, 180 degree sharp bend, bed shear stress, reynolds shear stress, secondary flow strength, vorticity, flow field*

1. Introduction

Natural rivers are characterized by complex geometries such as channel expansions and contractions, bends, and variable bed and bank roughness. These features are believed to create an unbalanced turbulent stress distribution along the cross-sectional plane, thus leading to the formation of secondary currents (Sin, 2010). Therefore, considering the effect of the secondary flow and velocity distribution on flow pattern in order to predict bed shear stress distribution in river and open channel bends is of high importance. Since bed shear stress parameter has a significant and fundamental role in sediment transport mechanism of rivers and alluvial channels, studying and determining bed shear stress has always been discussed in river engineering field. Accordingly, there have been a large number of studies conducted on secondary flow structure and shear stress distribution at bend routes. Thomson (1876) was the first to report the existence of spiral flow pattern in bend channels due to interactions between the secondary flow and lack of consistency in velocity profile along the channel. Mockmore (1943) conducted experiments on two 180 degree bends, measured longitudinal velocity profiles, and concluded that there is more flow near the inner wall than near the outer wall. Moreover, He found flow pattern in the bend, and demonstrated that velocity is distributed through the cross section in a way that if tangential velocity is multiplied by radius of curvature, the result will be constant. Shukry (1950) studied flow in the river's bend, and introduced a criterion for the strength of the secondary flow. He concluded that in a bend, the kinetic energy of the lateral flow is smaller than that of the longitudinal orientation. Rozovskii (1957) offered a relation for the determination of a specific length for when the secondary flow has the maximum strength. Based on such relation, it was concluded that in order to develop secondary flow, a bend with a central angle of at least 100 degrees is required for shallow flumes, and a 180 degree bend for deep ones. He also observed that assuming logarithmic distribution for velocity profile will lead to favorable results. Ippen and Drinker (1962) examined shear stress and velocity distributions in trapezoidal meandering bends with varying entrance conditions. They trickled some color into water, and observed that the color string at the channel bed would orient towards the internal bend, while that on the water surface oriented towards the outer bank. They called such phenomenon the effect of wall friction on flow field. They also determined a relationship between radius of curvature and

*Assistant Professor of Hydraulic Structures, Dept. of Civil Engineering, Persian Gulf University, Bushehr, Iran (Corresponding Author, E-mail: Vaghefi@pgu.ac.ir)
**M.Sc Graduated Student of Hydraulic Structures, Dept. of Civil Engineering, Persian Gulf University, Bushehr, Iran (E-mail: m.akbari@pgu.ac.ir)
***Assistant Professor, Dept. of Civil Engineering, Persian Gulf University, Bushehr, Iran (E-mail: fiouz@pgu.ac.ir)

maximum shear stress. Leschziner and Rodi (1979) numerically simulated the turbulent flow in a 180 degree sharp bend by using k-ε model. They assumed the absence of hydraulic jump and flow separation. They observed that the maximum velocity tends to occur towards the external bend closer to the end of the bend. Nouh and Townsend (1979) investigated the effect of the secondary flow on the bed shear stress distribution, and the results suggested that not only does the effect of the generated secondary flow remain after the bend exit, but it also continues towards the downstream bend. Odgaard (1986) presented a mathematical model in order to simulate bed changes in meander, alluvial rivers. He assumed the flow to be developed and modeled the changes in topography and longitudinal velocity using this model, and observed fluctuating behavior of the channel bed along the bend and how it decayed. Jian and McCorquadale (1998) undertook a 3D hydrodynamic modeling of the flow in the bend. The hydrodynamic model they provided was able to model the changes in free surface and bed topography. Wu *et al.* (2000) studied 3-D flow pattern, considering sediment as bed and suspended loads in a 180 degree bend. This model well predicted the secondary flow. They also determined the twist angle of velocity vector which was averaged, and concluded that at higher levels it is greater near the outer wall than in the sections on the opposite. Shams *et al.* (2002) carried out a numerical and experimental analysis in a bend flume, and concluded that the measured mean parameters of the flow resemble the results of the numerical model, but the turbulence parameters generated by the measurements differ from those results. Booij (2003) modeled the flow pattern in a 180 degree mild bend using Large Eddy Simulation Method (LES). He calculated the Reynolds stresses in the channel and compared the results of LES with them. The stresses can be used to examine the displacement of the longitudinal momentum and the effect of transporting the momentum of the secondary flow on longitudinal momentum. Blanckaert and Graf (2004) studied redistribution of velocity, boundary shear stress, and the form and features of bed topography in bend flumes. They determined bed topography in bend flumes by considering a central zone as a circulation cell, and using a semi 3D model. Yang (2005) studied the interaction among boundary shear stress, velocity distribution pattern and secondary flows in open channels. He applied the shear stress and velocity distribution to laminar, steady, and turbulent flows and stated the equations governing the Reynolds stress distribution and boundary shear stress. Ruther and Olsen (2005) simulated the secondary flow and transportation of sediment in a 90 degree narrow flume by using the k-ε turbulence model. The results of their simulation indicate that the direction of sediment transport depends on the direction of the shear stress near the bed. Roca *et al.* (2007) conducted an experimental study on scour and reduction of bed erosion in bend channels using a particular bed which resulted in a 40% reduction in scour. Zeng *et al.* (2008) carried out an investigation of the flow and sediment transport in bend channels with sharp slope on rigid and mobile beds. Studying the bed in two processes of scour and sedimentation at its initial and finishing stages, they concluded that quality improvement in turbulence models would result in a more accurate anticipation of sediment transport models. Abhari et al. (2010) conducted experimental and numerical studies of flow pattern in a 90 degree bend and concluded that streamlines at the level close to the bed orient to the inner wall, whereas those near water surface orient to the outer wall. Stoesser *et al*. (2010) computed turbulent flow in a meandering channel with two Computational Fluid Dynamics (CFD) codes (RANS and LES) solving the Navier-Stokes equations by employing different turbulence closure approaches. They compared the results obtained from the two codes with experimental data from a physical model study and showed that both LES and RANS simulation predicted the primary helical flow pattern in the meander as well as the occurrence of an outer-bank secondary cell. Khodashenas *et al.* (2010) studied the effects of vortex formation on the performance of orifice spillways using two physical models of the Karun III dam in Iran. They introduced three different classes of vortices (A, B, and C classes). The experiments showed that a strong vortex was formed (class A) with the decrease of the relative submerged depth to 3.7. Albayrak and Lemmin (2011) combined detailed ADVP, LSPIV, and hot-film measurements to analyze secondary current dynamics within the water column and at the free surface of an open-channel flow over a rough movable bed. They observed bottom shear stress obtained from hot-film measurements showing undulations in the spanwise direction. Morever, they found stronger bottom shear stresses in downwelling regions, and the weaker ones in neighboring upwelling regions. Uddin and Rahman (2012) carried out an experimental study of 3D flow and scour pattern by using ADCP velocimeter in the bend of the Jamuna River. They measured 3D velocity of the flow and shear stress near the river bed, and presented a model in order to predict erosion in the bend based on the processes of the flow. Finally, they compared the results with the real data recorded through their observations of the river. Kang (2013) numerically simulated turbulent flows and morphological changes in an open channel that had alternate vegetated zones by using a three-dimensional model. He observed that when the channel morphological changes were simulated with a series of floods, the initial rectangular channel became a compound channel and the flow pattern changed from a straight stream to a meandering stream. Yazdi *et al.* (2010) simulated the flow pattern around single spur dike in a straight route using k-ε model in Fluent software. They studied the effect of discharge, and length and angle of the spur dike on shear stress distribution. The results showed the maximum bed shear stress occurring in vertical spur dike rather than for spur dikes oriented upstream or downstream. Vaghefi *et al.* (2009-2012) placed the T-shaped spur dike in a 90 degree bend, and carried out several experimental studies on how the Froude number, the length of the spur dike, the position of the spur dike, the radius of curvature, etc., affected flow and scour pattern. They concluded that elongating the spur dike, shortening the wing of the spur dike, increasing Froude number,

and positioning the spur dike towards downstream will result in an increase in the dimensions of the scour hole. Prior to that, Vaghefi *et al.* (2014) had undertaken design and construction of a 180 degree sharp bend flume, which was the first 180 degree sharp bend flume in Iran. Through the Depth-Averaged method, they studied bed shear stress distribution along the bend and concluded that the maximum dimensionless bed shear stress occurred near the inner wall at the 40 degree angle.

Compared with other research studies carried out on 180 degree bends, this paper is innovative in conducting a complete experimental study on the mean and turbulent flow pattern in a 180 degree sharp open channel bend to determine bed shear stress distribution. Therefore, streamlines, maximum velocity distribution, vorticity, secondary flow strength, and bed shear stress distribution via the Turbulent Kinetic Energy, Modified Turbulent Kinetic Energy, and Reynolds shear stress methods (all of which are measured based on the turbulent flows) have been examined and analyzed.

2. Experimental Setup

The experiment was conducted in a bend with a 180 degree central angle in the Hydraulic Laboratory of Persian Gulf University in Bushehr, Iran. Fig. 1 presents a schematic 3D view of the flume and its parts in the laboratory. Various parts of the bend flume as well as their measures have been presented in the figure. The details of the flume bend section have also been shown in Fig. 2. As is observed, the flume is composed of a 6.5 meter long upstream and 5.1 meter long downstream straight reaches, both of which are connected via a 180 degree bend with an external and internal radius of curvature of 2.5 and 1.5 meters, respectively. According to Leschziner and Rodi (1979), this bend

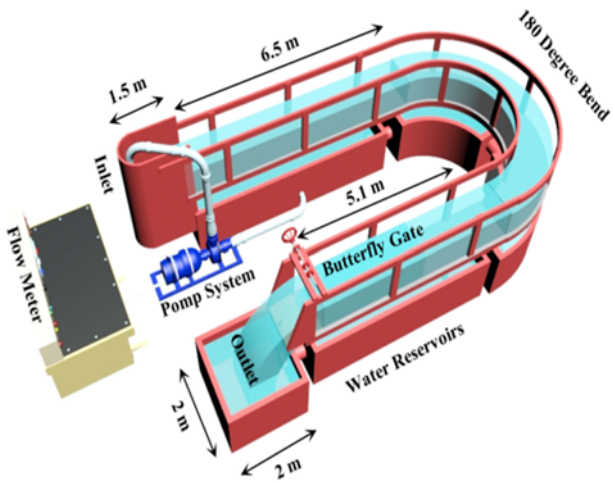

Fig. 1. The Schematic, 3D View of thE Laboratory Flume, Its Parts and Their Measures

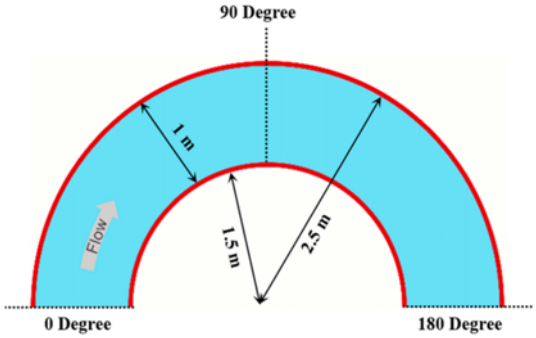

Fig. 2. The Details of the 180 Degree Sharp Bend Measures

is classified as a sharp bend. The flume is made of glass held in place with steel frames. Uniform sediments with a thickness of 1mm are glued to the flume bed in order to help determine roughness. The reservoirs underneath can hold water up to 20 m^3 to provide the water supply of the flume. The flow discharge is set at the beginning of the experiment using a flow meter, and is constant during the experiment. The depth of the flow is controlled by using the butterfly gate which had been installed at the end of the downstream reach. Geometric features of the flume, along with the hydraulic conditions governing the flow in the experiment, are presented in Table 1.

In Table 1;

Q is the discharge capacity of the flow, H water depth at the entrance to the bend, S the slope of the flume, Fr the Froude number, Re the Reynolds number, B the flume width, and R/B is the ratio of the central radius to channel width.

Vectrino 3D velocimeter, which is one of the most advanced ADV's (Acoustic Doppler Velocimeter), is utilized to measure velocity components, and determine the 3D flow pattern. One of the functions of the device is to measure the flow at a distance of 5 centimeters from the tip of its sensor (Nortek, 2009). Thus, the side looking probe measures the velocity near the water surface, and the down looking probe is used at other layers. The velocimeter was set at 25 Hz frequency, and the measurement of each point on the defined meshing took one minute to record data. 25 Hz is the maximum frequency acceptable for this software. It is considered as the frequency in conducting flow pattern experiments so as to obtain the largest number of collected flow velocity samples to achieve more accuracy in calculating the mean and fluctuating velocities based on the allotted time for flow velocity data collection and hence turbulent and mean flow pattern presentation. Therefore, at any point and in any direction, there was 1500 output velocity data, which were all averaged and filtered by Vectrino and Explorer V. In this experiment, 3D velocity profile was collected at 23 cross sections along the bend, and 6 depths, and 13 points were collected at each transverse axis.

Table 1. Geometric Features of the Flume, and the Hydraulic Conditions Governing the Flow

Depth of Flume	R/B	B	Re	Fr	S	H	Q
0.7 m	2	1 m	119000	0.34	0.001 %	0.2 m	95 L/s

3. Discussions of Results

3.1 Variations in Streamlines, and Velocity Contours

In order to provide an accurate evaluation of flow pattern variations in a 180 degree sharp bend, both the turbulent streamlines and velocity contours are presented in Figs. 3 to 5 in different cross sections, longitudinal sections, and plan views, respectively.

Figure 3 presents streamlines and contour of longitudinal velocity (V) in 0, 40, 80, 90, 130 and 180 degree cross sections. that velocity increases from the bed to water surface. After this cross section, centrifugal force is more effective. Hence, from the 10 degree cross section onward, there are secondary flows found at the width of the channel. As seen in Fig. 3(b), the effect of the secondary flow on flow pattern is evident at the 40 degree cross section, but there have been no vortices formed there yet. The maximum velocity of the flow has been thoroughly redirected towards the inner wall. Upon reaching the 80 degree cross section (Fig. 3(c)), the centrifugal force increases dramatically, and the secondary flow reaches the highest effect. Consequently,

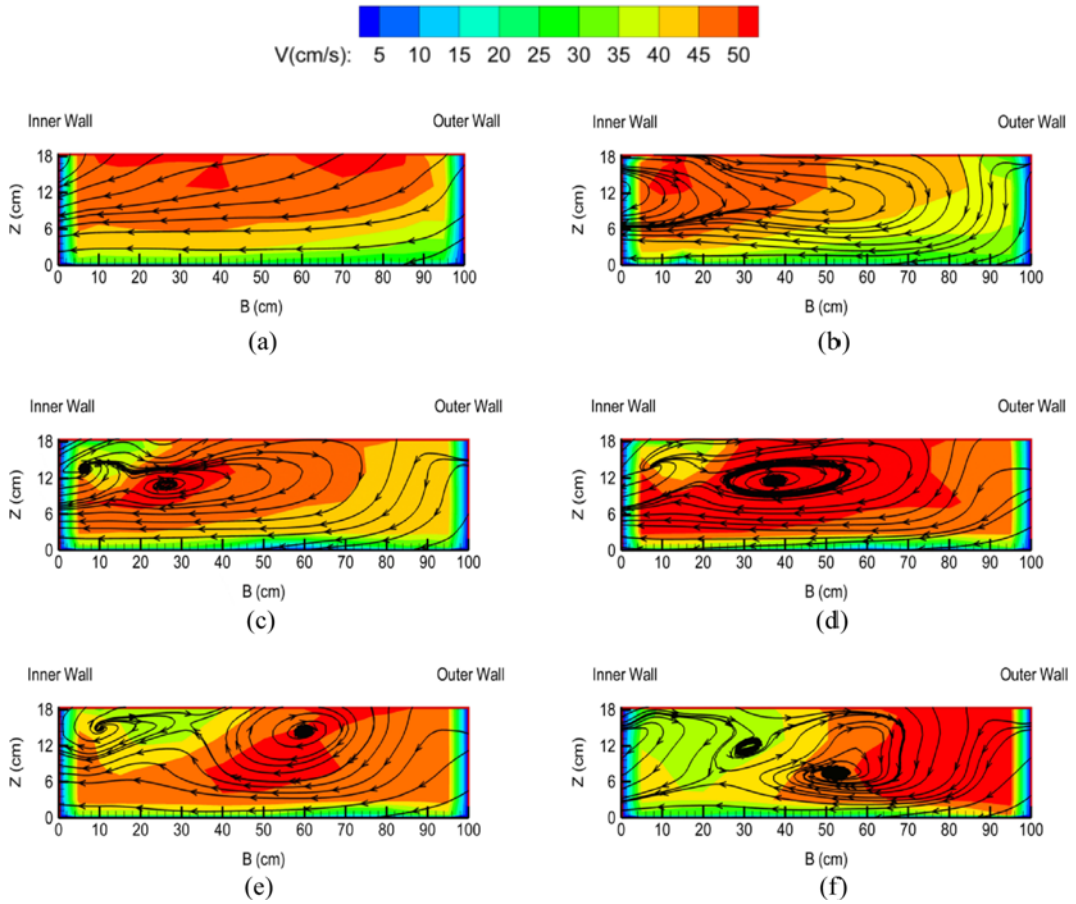

Fig. 3. Streamlines and Contours of Longitudinal Velocity in Different Cross Sections in a 180 Degree Sharp Bend at: (a) 0, (b) 40, (c) 80, (d) 90, (e) 130, and (f) 180 Degree Cross Sections

As is observed, no spiral flows are found at the initial cross section of the bend (Fig. 3(a)), and there are unidirectional radial flows oriented towards the inner wall. As suggested by Leschziner and Rodi (1979), such flows exist due to longitudinal positive and negative pressure gradients along inner and outer walls of the bend. In other words, since longitudinal acceleration increases about the internal bend, and drastically decreases at the external bend, the lateral flows from the external bend towards the internal bend are required to maintain the flow continuity. As demonstrated in the figure, velocity is not distributed much symmetrically at the width of the section, and the high velocity area is a bit inclined towards the inner wall. It can also be seen two circulation cells in the same direction can easily be detected near the bend's inner wall at distances of about 5% and 25% of the channel width from the inner wall. This phenomenon is depicted more extensively at the 90 degree cross section in Fig. 3(d). It is observed that a clockwise circulation flow called central circulation cell is formed at a distance of 38% of the channel width from the inner wall, at a level of 65% of the depth from the bed. Furthermore, there is another circulation flow in the same direction found at a distance of about 5% of the channel width from the internal bend. Investigation of the velocity contours at these sections (Figs. 3(c) and 3(d)) indicates that the high velocities exist in the area where the central circulation cell

is formed, which is extended from the mid-depth of the flow to the water surface. Blanckaert and Graf (2001), conducted some studies on flow pattern in a 120 degree sharp bend, reported the second circulation cell in the 60 degree cross section near the outer wall, and stated that the vortex is directed in the opposite direction of the main vortex. Further away on the route, after the second half of the bend (Fig. 3(e)), the secondary flow has less effect due to decrease in flow velocity and centrifugal force. As such, the vortex formation area moves to water surface, and the central vortex becomes smaller. Observed in Fig. 3(f), the secondary flows continue to run in the 180 degree cross section. As the flow passes through the bend exit, the velocity increases, and the secondary flows still exist. It can be seen that the central vortex approaches the channel bed. In other words, the flow is still under the influence of the bend, and has not been affected by the downstream straight route yet. Moreover, since the longitudinal pressure gradient is dominant, velocity transport phenomenon occurs, and the maximum velocity is redirected towards the outer wall of the channel. These results in Fig. 3(f) are consistent with those obtained from Leschziner and Rodi (1979) and Rozovskii's (1957) investigations.

Streamlines and contours of vertical velocity (W) are presented at longitudinal sections near the inner and the outer walls of the bend in Fig. 4 to study up flow and down flow streamlines along the bend. As can be seen in Fig. 4(a) (near the outer bank), most of the streamlines are down flow to 80% of the flow depth from the bed. Thereafter, and at higher layers, in the second half of the bend onward, they turn into up flow streamlines. Away from the outer wall area, by investigating the streamlines near the inner wall (Fig. 4(b)), it can be observed that the streamlines at layers as deep as 30% of the flow depth from the water surface are oriented down flow, whereas when they reach the bend apex area (the 75 degree angle ahead) until the end of the bend route they are oriented up flow. The changes in streamlines directions can be attributed to the formation of the clockwise vortices at various cross sections, both near the apex and after that (Figs. 3(c) to 3(f)). The effect of vortex formation is better realized in Fig. 4(b) (near the inner bank). In addition, the sharpness of the bend (R/B = 2) can be considered as another reason why the streamlines change direction and hit the channel wall. In Figs. 4(a) and 4(b), the positive and negative values of the vertical velocity component of the flow are also indicative of the up flow and down flow streamlines at these sections.

In Fig. 5, the streamlines and longitudinal velocity distribution of the flow are depicted in plan views at distances of 5% and 95% of the flow depth from the channel bed. As is seen in Fig. 5(a), the streamlines are inclined toward the inner wall of the bend all the way through the bend. The high velocity area also falls near the inner wall until it is redirected towards the outer wall of the bend at the end of the route. Investigation on the

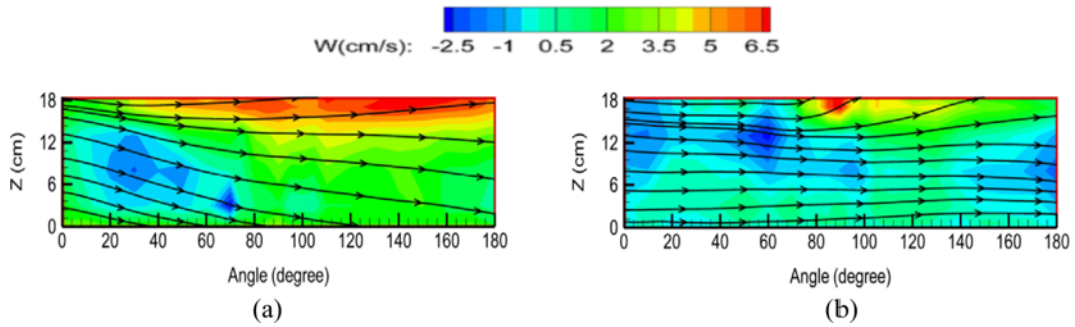

Fig. 4. Streamlines and Contours of Vertical Velocity at Various Longitudinal Sections at Distances of: (a) 5% and (b) 95% of the Channel width from the Outer Bank

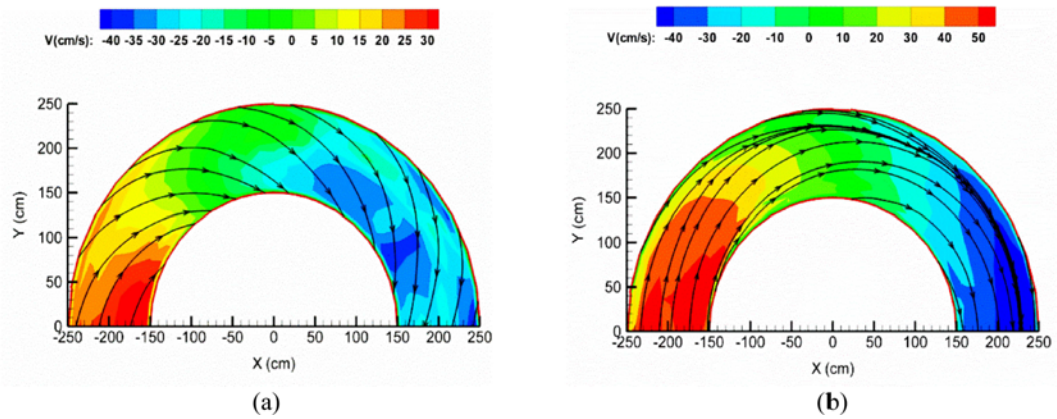

Fig. 5. Streamlines and Contours of Longitudinal Velocity at Different Plan Views at Distances of: (a) 5%, (b) 95% of the Flow Depth from the Bed

streamlines near the water surface (Fig. 5(b)) indicates that the streamlines are in the same direction as the bend curvature from the beginning to the mid-width of the channel. Thereafter, they are redirected towards the outer wall. The increase in flow depth, flow velocity and centrifugal force leads to a stronger secondary flow, and the streamlines are more likely to attack the outer bank. The area of the maximum velocity of the flow at the beginning and end of the route in the figure is quite justifiable considering the longitudinal pressure gradient being dominant in the sharp bend. A comparison between the flow velocity contours at two layers, one near the bed and the other near the water surface, indicates a 40% increase in flow velocity at the entrance of the bend.

3.2 Distribution of the Maximum Velocity Along the 180 Degree Sharp Bend

In Fig. 6, the maximum velocity path is depicted on its route at two different depths near the bed and water surface, along the 180 degree sharp bend. As seen in Fig. 6(a) and at the layer near the bed, the maximum velocity occurs at the entrance to the bend, near the inner bank, and it continues to be oriented towards the inner bank all along the bend. Leschziner and Rodi (1979) attributed this cause to the intensive lateral variations of longitudinal pressure gradient at the sharp bend entrance, because on the one hand, the formation of lateral slope results in negative pressure gradient and increases acceleration near the inner wall, and on the other hand, it causes positive pressure gradient and decreases acceleration near the external bend. However, further on the route, upon reaching around the bend exit, the maximum velocity is oriented towards the outer bank (these results can also be obtained by observing velocity contours in Figs. 5(a) and 3(f)). Such phenomenon occurs, as mentioned earlier, due to the bend sharpness, and consequently to the longitudinal pressure gradient's dominance over the secondary flow along the route. These observations seem to be adequately in accordance with the studies on two 180 degree bends conducted by Mockmore (1943) and those on a 180 degree bend with ratio of curvature radius to channel width equal to 1 done by Leschziner and Rodi (1979). Whilst investigating higher flow depths, the change in the location of the maximum velocity is evident. The maximum velocity path, as seen in Fig. 6(b), is inclined towards the internal bend at the first half of the bend, but around the apex and at the second half of the bend, it remains near the external bend all the way to the end of the route (Due to the increase in the secondary flow strength at this layer).

3.3 Comparison between the Secondary Flow Strength and Vorticity Along the Sharp Bend

There are two major criteria when investigating the secondary flow in bend routes, and they are discussed here on a 180 degree sharp bend. These criteria can help evaluate the secondary flow strength at different cross sections.

Shukry (1950) conducted some studies on flow in river bends, described the mechanism of the secondary flow and introduced the following criterion (Eq. (1)) for secondary flow strength to discuss the quantity of the phenomenon:

$$S_{xy} = \frac{K_{lateral}}{K_{main}} \tag{1}$$

In a specific cross section, the criterion includes the ratio of the lateral flow kinetic energy to the main flow kinetic energy. In Eq. (1), S_{xy} represents the secondary flow strength, whereas $K_{lateral}$ and K_{main} represent kinetic energy of the lateral flow and that of the main flow, respectively.

Using Eq. (2), secondary flow strength is defined as:

$$S_{xy} = \frac{\left(\frac{V_{xy}^2}{2g}\right)}{\left(\frac{V^2}{2g}\right)} \tag{2}$$

Where:

$$V_{xy} = (v^2 + w^2)^{0.5} \tag{3}$$

$$V = (u^2 + v^2 + w^2)^{0.5} \tag{4}$$

In Eqs. (3) and (4), u, v, and, w are velocity components along the length, width and depth of the channel, respectively, and g is the acceleration of gravity.

Another important and theoretical criterion introduced for the

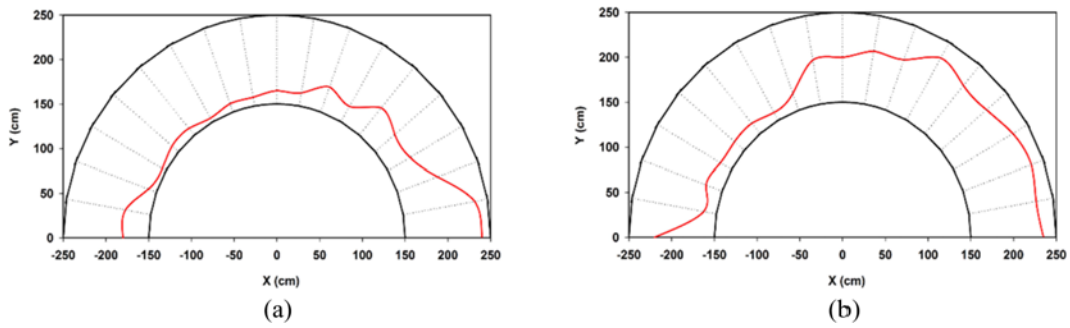

Fig. 6. Maximum Velocity Path at Various Depths Along the 180 Degree Sharp Bend at Distances of: (a) 5%, (b) 95% of the Flow Depth from the Bed

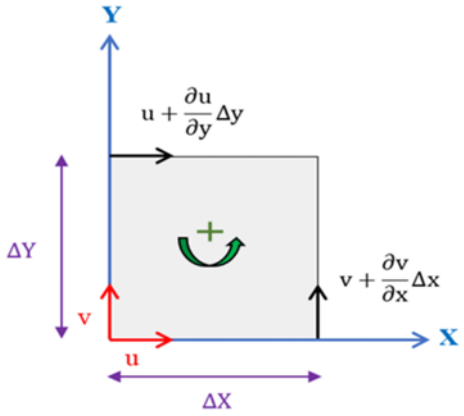

Fig. 7. The Diagram of a Cell's Circulation Around Perpendicular Axis

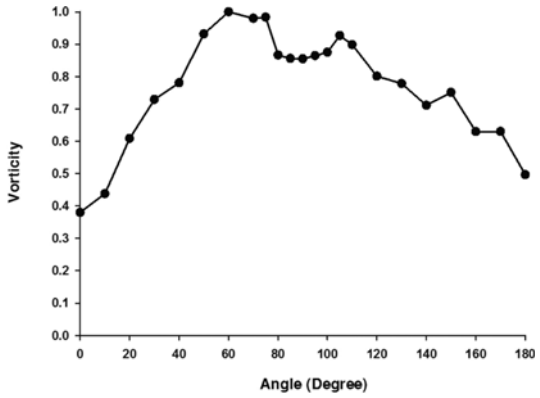

Fig. 9. Dimensionless Vorticity at Different Cross Sections Along the 180 Degree Sharp Bend

determination of the secondary flow effect on bend reaches is Vorticity Criterion. By definition, the net rate of a counterclockwise circulation of a cell as large as $\Delta x \times \Delta y$ around a perpendicular axis (total average of the circulation of Δy and Δx) is called "circulation", and according to Fig. 7, it is represented as Eq. (5) (Daily and Harleman, 1966).

$$\omega_z = \frac{1}{2}\left(\frac{\partial u}{\partial y} - \frac{\partial v}{\partial x}\right) \tag{5}$$

In this equation;

ω_z = Amount of circulation around the axis
u = Lateral velocity
v = Vertical velocity

Here, both methods are utilized to calculate the average amounts of the secondary flow strength via Shukry's method and vorticity at different cross sections along the 180 degree bend. The dimensionless values of the secondary flow strength and vorticity (the values which have become dimensionless by the maximum secondary flow strength and the maximum vorticity along the bend) are presented in Figs. 8 and 9, respectively. As depicted in Fig. 8, Shukry's method defines no significant secondary flow strength at the beginning of the bend due to longitudinal pressure gradient. However, affected by the increase in flow velocity and the centrifugal force, the secondary flow grows stronger thereafter, reaching the maximum extent equal to 7.7% near the apex of the bend at the 80 degree angle. The role the strong secondary flows play in the formation of two vortices in the same direction at this section is evident in Fig. 3(c). From the 80 degree location to the end of the bend, however, the secondary flow is gradually weakened due to decrease in flow velocity, and it can be observed in Figs. 3(d) to 3(f) that the central vortex has also become smaller. As mentioned earlier, at the end of the bend, despite the increase in flow velocity, the secondary flow continues to be weakened due to the dominance of the longitudinal pressure gradient. Naji *et al.* (2010) calculated the secondary flow strength via Shukry's method in a 90 degree bend (R/B = 3), and reported its maximum value for different Froude numbers at the 30 degree cross section. As is seen in Fig. 9, and with regards to elements circulation (vorticity), there is little circulation at the beginning of the route due to the effect of the flow entering the upstream route into the bend. However, from the 20 to 60 degree cross sections, the elements circulated more and more until they reached the maximum circulation equal to 3.3 1/s at the 60 degree location. Further on the route, the circulation decreases at most cross sections, and this is similar to the process the secondary flow strength went through in Shukry's method. Safarzadeh (2005), undertook a numerical investigation of the secondary flow strength along a 180 degree mild bend (R/B = 4.33) using the vorticity method, and concluded that the maximum vorticity occurs at 60 degree section. However, he reported increasing vorticity at the bend exit due to a vortex being formed in the opposite direction of the central vortex near the external bend. The results presented in Fig. 9 are very similar to those obtained from Rozovskii's (1957) in growth and depreciation of the secondary flow for a sharp bend where R/B = 1.

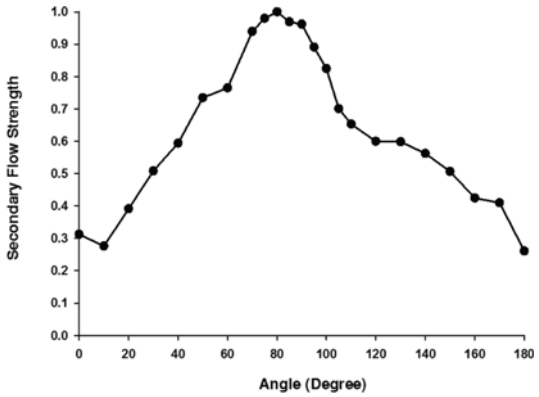

Fig. 8. Dimensionless Secondary Flow Strength Via Shukry's Method at Different Cross Sections Along the 180 Degree Sharp Bend

3.4 Bed Shear Stress Distribution Along the 180 Degree Sharp Bend

Shear stress parameter is one of the contributing factors in the

prediction of scour in mobile beds. Even though this paper assumes a rigid bed, bed shear stress distribution can to a large extent help with the qualitative understanding of scour pattern. Here, three different methods are used in order to measure bed shear stress: Reynolds, Turbulent Kinetic Energy (TKE), and Modified Turbulent Kinetic Energy (TKE-w') shear stress methods, all of which are measured based on the turbulent flows. Thereafter, equations used in the measurement of bed shear stress via these methods are described. When it is possible to collect velocity at turbulent boundary layer, the Reynolds shear stress and other mentioned methods are used taking the following equations into account.

Reynolds shear stress method Eq. (11) is applied to calculate bed shear stress at two layers of 5% and 15% of the flow depth from the bed (Barbhuiya and Dey, 2004).

$$\tau_b = (\tau_x^2 + \tau_y^2)^{0.5} \tag{11}$$

$$\tau_x = -\rho\left(\overline{w_l' u_l'} + \overline{v_l' u_l'}\right) \tag{12}$$

$$\tau_y = -\rho\left(\overline{v_l' u_l'} + \overline{v_l' w_l'}\right) \tag{13}$$

$$u_i' = u_i - \overline{u} \tag{14}$$

$$v_i' = v_i - \overline{v} \tag{15}$$

$$w_i' = w_i - \overline{w} \tag{16}$$

Where,

u_i, v_i and w_i represent the collected point velocity along the length, width and depth of the channel, respectively.

u_i', v_i' and w_i' represent the fluctuating velocity along the length, width and depth of the channel, respectively.

$\overline{u}_l$, $\overline{v}_l$, and $\overline{w}_l$ represent the mean velocities along the length, width, and depth of the channel, respectively.

The TKE method is a method for determination of bed shear stress, which is done through measuring three fluctuation velocity components, in accordance with Eq. (17) (Kim *et al*., 2000).

$$\tau_0 = C_1[0.5\rho(\overline{u'^2} + \overline{v'^2} + \overline{w'^2})] \tag{17}$$

Where, C_1 is a constant, and based on the investigations carried out by researchers, it equals 0.19.

Kim *et al.* (2000), modified the Turbulent Kinetic Energy method, and only used the vertical component of velocity fluctuations to measure bed shear stress. They did this because there was measurement error in horizontal components of velocity fluctuations when using instruments like ADV, and the error in vertical velocity fluctuations is much less than that in the horizontal one. The researchers offered the following equation for measuring bed shear stress (Kim *et al.*, 2000):

$$\tau_0 = C_2[\rho\overline{w'^2}] \tag{18}$$

Where, C_2 is a constant, and based on the investigations carried out by researchers, it equals 0.9.

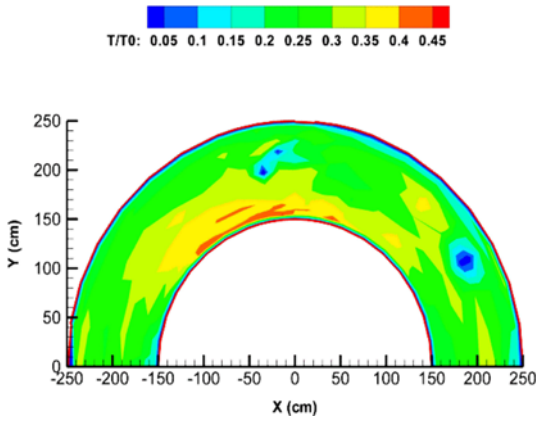

Fig. 10. Dimensionless Bed Shear Stress Distribution Along the 180 Degree Sharp Bend Via the TKE Shear Stress Method at a Distance of 5% of the Depth from the Bed

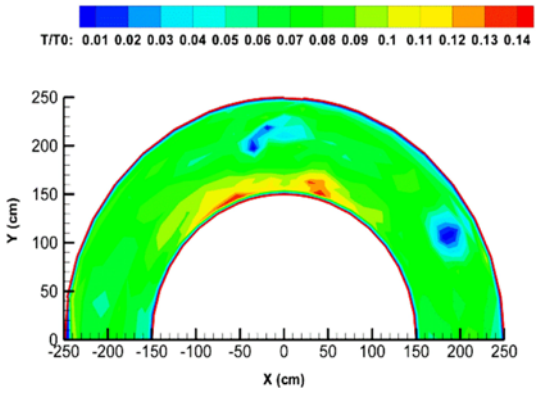

Fig. 11. Dimensionless Bed Shear Stress Distribution Along the 180 Degree Sharp Bend Via the TKE-w' Shear Stress Method at a Distance of 5% of the Depth from the Bed

Thus, 3D flow velocities at 5% of the flow depth from the bed are collected to calculate the TKE and TKE-w' methods, and the determination of Reynolds shear stress at two layers of 5% and 15% of the flow depth from the bed. The values obtained from these methods have become dimensionless by shear stress at the upstream straight route ($\tau = \rho u^2$). The dimensionless bed shear stress distribution via the TKE, TKE-*w*', and Reynolds shear stress methods in a 180 degree sharp bend (R/B = 2) are displayed in Figs. 10 to 13.

Figure 10 indicates that in the TKE method, the maximum dimensionless shear stress occurs around the bend entrance, near the inner wall and after that around the apex of the bend. Moreover, the dimensionless shear stress has increased at the end of the route in a very small area in the bend exit. The way the bed shear stress is distributed in Fig. 10 is easily predictable considering the maximum velocity distribution presented in Fig. 6, the analyses given on streamlines, the longitudinal pressure gradient's dominance on the route, the effect of the secondary flow strength near the apex of the bend and the velocity distribution pattern near the inner wall in Figs. 3(c) and 3(d). As is seen in Fig. 11, the bed shear stress distribution in the TKE-w'

is very similar to Fig. 10, except that firstly, there is no shear stress found at the bend exit, and secondly, the stress in this method is less than that in the first method. A comparison between Figs. 10 and 11 concludes that the bed shear stress distribution measured by the TKE method covers a wider range of the shear stress values. Also, the maximum bed shear stress in the TKE-w' method is almost 30% of that in the TKE method. This is due to vertical component of velocity fluctuations being much smaller than the other two velocity fluctuations. Since only the vertical component of velocity is used in the TKE-w' method in calculating shear stress, its values are smaller than those of bed shear stress in TKE method. As Figs. 12 shows, the bed shear stress distribution in the Reynolds shear stress method is greatly disorganized due to the velocimeter's sensitivity at the layers near the bed (the turbulent boundary layer at a distance of 5% of the depth from the bed). In spite of the maximum bed shear stress occurring near the inner wall from the beginning to the end of the bend, near the bend exit, the maximum shear stress is transported to the areas near the outer wall. The location of the maximum dimensionless shear stress in Fig. 12 is observed at the 40 degree cross section. Comparison between the three mentioned methods in determining bed shear stress at a distance of 5% of the depth flow from the bed indicates that the TKE and TKE-w' methods show smaller values in bed shear stress calculation compared to the Reynolds method. However, the Reynolds and TKE shear stress methods have to some extent similar results with respect to both the shear stress distribution and the maximum shear stress location at the beginning and at the end of the bend. The regular distribution of the shear stress in Fig. 13 is more obvious than that of Fig. 12. As seen, in Fig. 13 the maximum shear stress location has distanced compared to its primary location in Fig. 12, reaching the 60 degree angle. A stronger secondary flow and displacement of the maximum shear stress area happen due to an increase in the flow depth from the bed and consequently in velocity, centrifugal force. Figs. 8 and 9 also specify that the maximum secondary flow strength and vorticity occur in an area between the 60 and 100 degree angles, which is actually the area in the middle of and around the bend apex. In other words, the

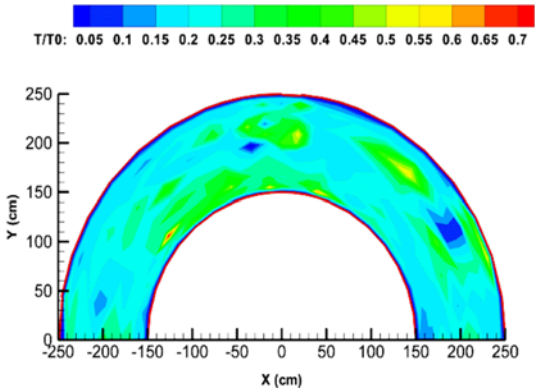

Fig. 12. Dimensionless Bed Shear Stress Distribution Along the 180 Degree Sharp Bend Via the Reynolds Shear Stress Method at a Distance of 5% of the Depth from the Bed

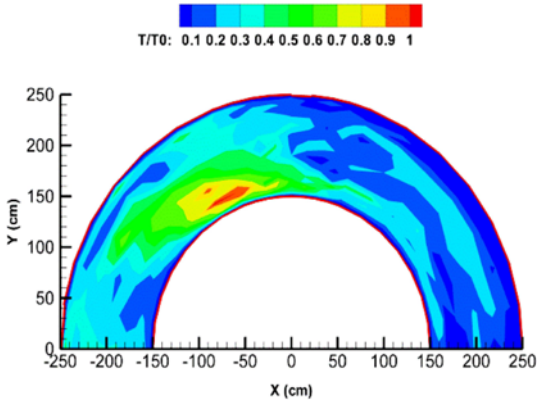

Fig. 13. Dimensionless Bed Shear Stress Distribution Along the 180 Degree Sharp Bend Via the Reynolds Shear Stress Method at a Distance of 15% of the Depth from the Bed

different locations of the maximum shear stress at two layers near the bed displays that an increase in the flow depth makes the maximum shear stress area distant from the bend entrance (where the effect of longitudinal pressure gradient is remarkable). As a result of a decrease in the longitudinal pressure gradient, and in fact dominating the secondary flows over the longitudinal pressure gradient, the maximum shear stress inclines towards the bend apex area, where the secondary flows have a great effect. Moreover, the variation in the secondary flow strength within a 20-100 degree interval (Figs. 8 and 9) explains the reason why the bed shear stress is formed and distributed near the inner wall in Figs. 10 to 13. Odgaard and Bergs (1988) have also referred to the existence of two distinct scour holes at the first half (the 55 degree cross section) and second half exit in their studies on a 180 degree mild bend with mobile bed. Begin (1986) and Yen and Ho (1990) reported that if R/B is less than 3.5 in a bend, two maximum stress areas can be found: one at the bend exit near the outer wall, and the other at the bend entrance near the inner wall. However, when R/B is too little, about 1.5, the shear zone entirely falls into the inner wall area. Therefore, based on the results obtained from the experiments conducted in a number of research studies, the factors affecting bed shear stress in river bends can be presented considering the curvature ratio of the bend (R/B), velocity distribution at the bend entrance section, central angle of the bend, the ratio of channel width to flow depth, the Reynolds number, the Froude number, and bed roughness factor. Under the experiment's conditions, the observations and results of the bed shear stress distribution obtained via these methods mentioned are consistent with those from the investigations carried out in these research reviews.

The Reynolds shear stress values shown in Figs. 12 and 13 for some of the compared points are presented in Table 2. In this table, represents the cross section at which the measurement is carried out, L the distance from the outer bank, R the radial distance from the bend center, and X and Y the coordination of the points in x- and y- directions in Cartesian system sequentially. It can be seen at some points in the field (e.g., B, D, F, I, S, U, W, Z,

Table 2. Comparison between Dimensionless Bed Shear Stress Values at Two Different Depth Layers Near the Bed Via the Reynolds Shear Stress Method

Name of Point	θ (Degree)	L (cm)	R (cm)	X (cm)	Y (cm)	τ_b/τ_0 z = 0.5 cm	τ_b/τ_0 Z = 3 cm
A	0	10	240	-240.00	0.00	0.30	0.31
B	0	70	180	-180.00	0.00	0.26	0.25
C	10	15	235	-231.43	40.81	0.28	0.33
D	10	85	165	-162.49	28.65	0.23	0.22
E	20	30	220	-206.73	75.24	0.23	0.32
F	20	50	200	-187.94	68.40	0.16	0.17
G	30	70	180	-155.89	90.00	0.24	0.45
H	30	40	210	-181.87	105	0.23	0.68
I	30	90	160	-138.56	80.00	0.20	0.21
J	40	40	210	-160.87	134.99	0.31	0.50
K	40	85	165	-126.40	106.06	0.73	0.39
L	50	50	200	-128.56	153.21	0.41	0.62
M	50	85	165	-106.06	126.40	0.32	0.72
N	60	85	165	-82.50	142.89	0.31	1.04
O	60	70	180	-90	155.88	0.29	0.95
P	70	20	230	-78.66	216.13	0.28	0.30
Q	70	85	165	-56.43	155.05	0.49	0.99
R	70	80	170	-58.14	159.75	0.37	0.9
S	75	10	240	-62.12	231.82	0.16	0.17
T	75	85	165	-42.71	159.38	0.27	0.89
U	80	10	240	-41.68	236.35	0.20	0.21
V	80	95	155	-26.92	152.65	0.31	0.60
W	80	40	210	-36.47	206.81	0.30	0.31
X	85	85	165	-14.38	164.37	0.33	0.71
Y	85	95	155	-13.51	154.41	0.50	0.56
Z	90	30	220	0.00	220.00	0.33	0.34
AA	90	95	155	0.00	155.00	0.35	0.41
BA	95	20	230	20.05	229.12	0.20	0.19
CA	95	90	160	13.94	159.39	0.27	0.64
DA	95	70	180	15.69	179.32	0.21	0.22
EA	100	70	180	31.26	177.27	0.20	0.12
FA	100	40	210	36.47	206.81	0.17	0.19
GA	105	10	240	62.12	231.82	0.16	0.17
HA	105	85	165	42.71	159.38	0.37	0.60
IA	110	20	230	78.66	216.13	0.21	0.31
JA	110	40	210	71.82	197.34	0.17	0.17
KA	120	80	170	85.00	147.22	0.22	0.44
LA	120	50	200	100.00	173.21	0.19	0.20
MA	130	40	210	134.99	160.87	0.33	0.21
NA	130	90	160	102.85	122.57	0.27	0.24
OA	140	30	220	168.53	141.41	0.26	0.30
PA	140	70	180	137.89	115.70	0.28	0.30
QA	150	15	235	203.52	117.50	0.38	0.06
RA	150	90	160	138.56	80	0.19	0.29
SA	160	80	170	159.75	58.14	0.19	0.17
TA	160	30	220	206.73	75.24	0.20	0.22
UA	170	60	190	187.11	32.99	0.24	0.17
VA	170	40	210	206.81	36.47	0.19	0.19
WA	180	50	200	200.00	0.00	0.25	0.27
XA	180	90	160	160.00	0.00	0.16	0.17

BA, DA, FA, JA, LA, VA, and WA Points) that the shear stress values obtained from the Reynolds shear stress method at two different layers near the bed are similar to each other. But a number of researchers, including Biron *et al*. (2004), Bagherimeyab *et al.* (2008), and Bagherimiyab and Lemmin (2013) have conducted studies on the difference in the Reynolds shear stress method at two different layers near the bed by investigating straight channels, and hence reported an increase in bed shear stress from water surface to bed; Whereas, it was observed that the deeper the depth from the bed, the greater the Reynolds stress. According to the data given in Table 2, in most of the presented points (note the stress values at H, K, M, N, O, Q, R, T, V, X, HA, KA, and QA Points), the bed shear stress distribution in the 180 degree sharp bend in depth has either become disorderly or experienced increased shear stress. This can be attributed to transverse flows and bed roughness and their effect on the flow turbulence. Also of note is that the velocimeter devices such as ADV, ADVP, etc., used also by other researches to measure flow velocity does not provide highly accurate measurements at the layers too close to the bed (depth of less than 10% of the flow depth from the bed); Consequently, they indicate shear stress reduction rather than shear stress increase at the layers near the bed.

4. Conclusions

The experimental study presented in this paper has evaluated and analyzed streamlines, velocity distribution variations, the maximum velocity path, the secondary flow strength, vorticity, and bed shear stress using three methods in order to investigate the parameters governing flow pattern and bed shear stress distribution in a 180 degree sharp bend. It was observed from the streamlines drawn in cross sections that there are two persistent clockwise vortexes formed. One is at the center (primary vortex), and the other near the inner wall of the bend (secondary vortex) from the bend apex to the bend exit. In these cross sections the primary vortex becomes smaller due to the decrease in the secondary flow strength. Since the longitudinal pressure gradient is dominant along the bend, at the layer near the bed, the maximum velocity always occurs along the inner wall of the bend until it is transported towards the outer wall at the bend exit. The results from the calculation of the maximum secondary flow strength along the bend using Shukry's method and vorticity suggest that the maximum strength of the secondary flow is found at the first half of the bend, and equals 7.7%, and 3.3 1/s at the 60 and 80 degree cross sections, respectively. From what had been calculated for bed shear stress via the TKE, TKE-*w*', and the Reynolds shear stress methods at a distance of 5% of the flow depth from the bed, it was seen that the maximum dimensionless bed shear stress in these methods occurred around the bend entrance, near the inner wall and after that around the apex of the bend. Moreover, the TKE and TKE-w' methods showed smaller values in bed shear stress calculation compared to the Reynolds method. Comparison of the Reynolds shear stress method at two depth layers indicated that at lower depth, maximum shear stress occurred at the 40 degree cross section, whereas at a distance of 15% of the flow depth from bed, it occurred at the 60 degree cross section, again near the inner wall.

References

Abhari, M. N., Ghodsian, M., Vaghefi, M., and Panahpur, N. (2010). "Experimental and numerical simulation of flow in a 90 bend." *Flow Measurement and Instrumentation*, Vol. 21, No. 3, pp. 292-298, DOI: 10.1016/j.flowmeasinst.2010.03.002.

Albayrak, I. and Lemmin, U. (2011). "Secondary currents and corresponding surface velocity patterns in a turbulent open-channel flow over a rough bed." *Journal of Hydraulic Engineering*, Vol. 137, No. 11, pp. 1318-1334, DOI: 10.1061/(ASCE)HY.1943-7900.0000438.

Bagherimeyab, F., Albayrak, I., and Lemmin, U. (2008). *Bed shear velocity estimates in rough open channel flow obtained from Acoustic Doppler Velocity Profiler data and direct bed shear stress measurements*, The River flow conference, Izmir, Turkey, pp. 151-159.

Bagherimiyab, F. and Lemmin, U. (2013). "Shear velocity estimates in rough-bed open-channel flow." *Earth Surface Processes and Landforms*, Vol. 38, No. 14, pp. 1714-1724, DOI: 10.1002/esp.3421.

Barbhuiya, A. K. and Dey, S. (2004). "Measurement of turbulent flow field at a vertical semicircular cylinder attached to the sidewall of a rectangular channel." *Flow Measurement and Instrumentation*, Vol. 15, No. 2, pp. 87-96, DOI: 10.1016/j.flowmeasinst.2003.11.002.

Begin, Z. E. B. (1986). "Curvature ratio and rate of river bend migration-update." *Journal of Hydraulic Engineering*, ASCE, Vol. 112, No. 10, pp. 904-908, DOI: 10.1061/(ASCE)0733-9429(1986) 112:10(904).

Biron, P. M., Robson, C., Lapointe, M. F., and Gaskin, S. J. (2004). "Comparing different methods of bed shear stress estimates in simple and complex flow fields." *Earth Surface Processes and Landforms*, Vol. 29, No. 11, pp. 1403-1415, DOI: 10.1002/esp.1111.

Blanckaert, K. and Graf, W. H. (2001). "Mean flow and turbulence in open-channel bend." *Journal of Hydraulic Engineering,* ASCE, Vol. 127, No. 10, pp. 835-847, DOI: 10.1061/(ASCE)0733-9429(2001) 127:10(835).

Blanckaert, K. and Graf, W. H. (2004). "Momentum transport in sharp open-channel bends." *Journal of Hydraulic Engineering*, ASCE, Vol. 130, No. 3, pp. 186-198, DOI: 10.1061/(ASCE)0733-9429 (2004)130:3(186).

Booij, R. (2003). "Measurements and large eddy simulations of the flows in some curved flumes." *Journal of Turbulence*, Vol. 4, No. 8, pp. 1-17, DOI: 10.1088/1468-5248/4/1/008.

Daily, W. and Harleman, D. (1966). *Fluid dynamics*, Addison-Wesley Publishing Company.

Ghodsian, M. and Vaghefi M. (2009). "Experimental study on scour and flow field in a scour hole around a T-shaped spur dike in a 90° bend." *International Journal of Sediment Research*, Vol. 24, No. 2, pp. 145-158, DOI: 10.1016/S1001-6279(09)60022-6.

Ippen, A. T. and Drinker, P.A. (1962). "Boundary shear stresses in curved trapezoidal channels." *Journal of the Hydraulics Division*, ASCE, Vol. 88, No. HY5, pp. 143-179.

Jian, Y. and McCorquadale, J. A. (1998). "Simulation of curved open channel flows by 3D hydrodynamic model." *Journal of Hydraulic Engineering*, ASCE, Vol. 124, No. 7, pp. 687-698.

Kang, H. (2013). "Flow characteristics and morphological changes in open-channel flows with alternate vegetation zones." KSCE Journal of Civil Engineering, KSCE, Vol. 17, No. 5, pp. 1157-1165, DOI:

10.1007/s12205-013-0346-5.

Khodashenas, S. R., Roshan, R., Sarkardeh, H., and Azamathulla, H. M. (2010). "Vortex study at orifice spillways of Karun III dam." *Dam Engineering*, Vol. 21, No. 2, pp. 131-142.

Leschziner, M. A. and Rodi, W. (1979). "Calculation of strongly curved open channel flow." *Journal of the Hydraulics Division*, ASCE, Vol. 105, No. 10, pp. 1297-1314.

Mockmore, C. E. (1944). "Flow around bends in stable channels." *Transactions of the American Society of Civil Engineers*, ASCE, Vol. 109, pp. 593-618.

Nortek, A. S. (2009). *Vectrino velocimeter user guide*, Nortek AS.

Nouh, M. and Townsend, R. D. (1979). "Shear-stress distribution in stable channel bends." *Journal of the Hydraulics Division*, ASCE, Vol. 105, No. 10, pp. 1233-1245.

Odgaard, A. J. (1986). "Meander flow model. I: Development." *Journal of Hydraulic Engineering*, ASCE, Vol. 112, No. 12, pp. 1117-1135, DOI: 10.1061/(ASCE)0733-9429(1986)112:12(1117).

Odgaard, A. J. and Bergs, M. A. (1988). "Flow processes in a curved alluvial channel." *Water Resources Research*, Vol. 24, No. 1, pp. 45-56.

Roca, M., Martín-Vide, J. P., and Blanckaert, K. (2007). "Reduction of bend scour by an outer bank footing: Footing design and bed topography." *Journal of Hydraulic Engineerin*g, ASCE, Vol. 133, No. 2, pp. 139-147, DOI: 10.1061/(ASCE)0733-9429(2007) 133:2(139).

Rozovskii, I. L. (1957). *Flow of water in bend of open channel,* Academy of Sciences of the Ukrainian SSR, Institute of Hydrology and Hydraulic Engineering.

Ruther, N. and Olsen, N. R. (2005). "Three-dimensional modeling of sediment transport in a narrow 90 channel bend." *Journal of Hydraulic Engineering*, ASCE, Vol. 131, No. 10, pp. 917-920, DOI: 10.1061/(ASCE)0733-9429(2005)131:10(917).

Safarzadeh, G. A. (2005). *Numerical simulation of flow pattern at lateral intake in 180 degree bend*, M.Sc. thesis, Tarbiat Modares University, Tehran, Iran. (In Persian)

Shams, M., Ahmadi, G., and Smith, D. H. (2002). "Computational modeling of flow and sediment transport and deposition in meandering rivers." *Advances in Water Resources*, Vol. 25, No. 6, pp. 689-699, DOI: 10.1016/S0309-1708(02)00034-9.

Shukry, A. (1950). "Flow around bends in an open flume." *Transactions of the American Society of Civil Engineers*, ASCE, Vol. 115, pp. 751-779.

Sin, K. S. (2010). *Methodology for calculating shear stress in a meandering channel*, M.Sc. thesis, Colorado State University, Colorado, United States.

Stoesser, T., Ruether, N., and Olsen, N. R. B. (2010). "Calculation of primary and secondary flow and boundary shear stresses in a meandering channel." *Advances in Water Resources,* Vol. 33, No. 2, pp. 158-170, DOI: 10.1016/j.advwatres.2009.11.001.

Thomson, J. (1876). "On the origin of windings of rivers in alluvial plains." *Proceedings of the Royal Society*, Vol. 25, pp. 5-8.

Uddin, M. N. and Rahman, M. M. (2012). "Flow and erosion at a bend in the braided Jamuna River." *International Journal of Sediment Research*, Vol. 27, No. 4, pp. 498-509, DOI: 10.1016/S1001-6279 (13)60008-6.

Vaghefi, M., Akbari, M. and Fiouz, A. R. (2014). "Experimental investigation on bed shear stress distribution in a 180 Degree Sharp bend by using Depth-Averaged Method." *International Journal of Scientific Engineering and Technology*, Vol. 3, No. 7, pp. 962-966.

Vaghefi, M., Ghodsian, M., and Salehi Neyshaboori, S. A. A. (2009). "Experimental study on the effect of a T-shaped spur dike length on scour in a 90 channel bend." *Arabian Journal for Science and Engineering*, Vol. 34, No. 2B, pp. 337-348.

Vaghefi, M., Ghodsian, M., and Adib, A. (2012). "Experimental study on the effect of froude number on temporal variation of scour around a t shaped spur dike in a 90 Degree Bend." *Applied Mechanics and Materials*, Vol. 147, pp. 75-79, DOI: 10.4028/www.scientific.net/ AMM.147.75.

Vaghefi, M., Ghodsian, M., and Neyshabouri, S. A. A. (2012). "Experimental study on scour around a T-shaped spur dike in a channel bend." *Journal of Hydraulic Engineering*, Vol. 138, No. 5, pp. 471-474, DOI: 10.1061/(ASCE)HY.1943-7900.0000536

Wu, W., Rodi, W., and Wenka, T. (2000). "3D numerical modeling of flow and sediment transport in open channels." *Journal of Hydraulic Engineering*, ASCE, Vol. 126, No. 1, pp. 4-15, DOI: 10.1061/ (ASCE)0733-9429(2000)126:1(4).

Yang, S. Q. (2005). "Interactions of boundary shear stress, secondary currents and velocity." *Fluid Dynamics Research*, Vol. 36, No. 3, pp. 121-136, DOI: 10.1016/j.fluiddyn.2005.01.002.

Yazdi, J., Sarkardeh, H., Azamathulla, H. M., and Ghani, A. A. (2010). "3D simulation of flow around a single spur dike with free-surface flow." *International. Journal of River Basin Management*, Vol. 8, No. 1, pp. 55-62, DOI: 10.1080/15715121003715107.

Yen, C. L. and Ho, S. Y. (1990). "Bed evolution in channel bends." *Journal of Hydraulic Engineering*, ASCE, Vol. 116, No. 4, pp. 544-562, DOI: 10.1061/(ASCE)0733-9429(1990)116:4(544).

Zeng, J., Constantinescu, G., Blanckaert, K., and Weber, L. (2008). "Flow and bathymetry in sharp open-channel bends: Experiments and predictions." *Water Resources Research*, Vol. 44, No. 9, pp. W09401.1-W09401.22, DOI: 10.1029/2007WR006303.